THE JOURNAL OF PHYSICAL CHEMISTRY B
A JOURNAL OF THE AMERICAN CHEMICAL SOCIETY

Editors' Choice
Open Access

pubs.acs.org/JPCB

Article

Metadensity Functional Learning for Classical Fluids: Regularizing with Pair Correlations

Published as part of The Journal of Physical Chemistry B special issue "Classical Density Functional Theory in Physical Chemistry".

Stefanie M. Kampa, Florian Sammüller, and Matthias Schmidt*

Cite This: https://doi.org/10.1021/acs.jpcb.6c01662

Read Online

ACCESS | Metrics & More | Article Recommendations

ABSTRACT: We investigate and exploit consequences of the recent neural metadensity functional theory by [Kampa, S. M. et al. *Phys. Rev. Lett.* **2025**, *134*, 107301] for describing the physics of inhomogeneous fluids. The metadensity dependence on the pair potential is relevant for soft matter design and Henderson inversion, and it allows one to change the pair potential on the fly at the prediction stage. Here we consider one-dimensional systems with short-ranged (truncated) interparticle forces and draw on the functional pair potential dependence to investigate "metadirect" routes toward the bulk fluid pair correlation structure. Classical density functional theory provides the required functional relationships. Efficient variational calculus is implemented by neural functional line integration and automatic differentiation. We regularize local learning of neural functionals by comparing the pair structure from different routes. Thereby, results from metadirect functional differentiation are matched against accurate test particle data from an initial locally trained metadensity functional. Accessing the pair structure via the metadensity functional dependence circumvents Ornstein–Zernike inversion, and it is based on first principles.

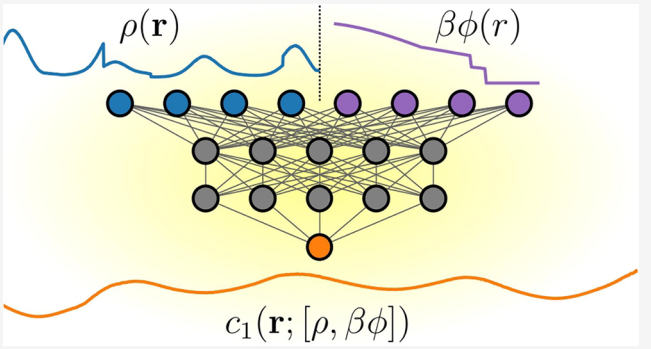

1. INTRODUCTION

The use of machine learning has a transformative effect on the fundamental sciences. The specific realm of soft matter research provides a clear-cut testbed for the integration of the technology into first-principles-based theoretical work. Classical density functional theory[1−5] supplies suitable equilibrium cornerstones, including the exact Mermin-Evans minimization principle,[2,6] the Euler−Lagrange equation as the basis for practical implementations, and the hierarchy of direct correlation functionals that emerge via functional differentiation. Associated Ornstein−Zernike and test-particle routes give access to correlation and response functions. A broad range of statistical mechanical sum rules interconnect and constrain the formal objects.[7−12]

As the classical version shares an analogous theoretical structure with quantum density functional theory,[5] it plays arguably a similarly promising role in the age of artificial intelligence. In particular the significant advantages in the generation of training data for any underlying *classical* particle-based system are noteworthy. A wide array of both standard and advanced particle-based simulation methods, such as Monte Carlo and molecular dynamics schemes, give direct access to the required averages and, perhaps even more importantly, they can be tailored flexibly toward the specific learning target and training strategy[13−22] (we provide an overview of further examples below).

A significant variety of different machine learning strategies for classical density functional theory has been put forward.[19,23−37] In particular the *local learning* method by Sammüller et al.[13,38] has proved to be both simple in practical use as well as highly adaptable to a considerable array of first-principles-based research goals.[13−18,20,21] The method allows one to use simulation data as an immediate basis for the accurate training of neural functionals. In contrast to "pure" simulation work, i.e., computing averages of interest via sampling under prescribed conditions, the neural method allows one to extract constructively the *functional* relationships that are inherent in the statistical mechanics and thus

Received: March 12, 2026
Revised: April 17, 2026
Accepted: April 30, 2026

imprinted in the training data. Functional relationships are high-dimensional in character, as they involve maps between function spaces. Hence traditional fitting methods are poorly equipped for making progress. In contrast neural networks and artificial intelligence methods are highly efficient in dealing with high-dimensional data.

Classical density functional theory offers a wide gamut of theoretical structure that can be exploited in practical machine learning applications to investigate diverse physical effects within a consistent theoretical framework. We give an overview of examples in the following. A locally trained hard sphere neural functional[13] was shown to surpass in accuracy Rosenfeld's fundamental measure theory for hard spheres[39] in its state-of-the-art White Bear Mk II version.[40] Thermally trained density functionals were shown to predict accurately the liquid−gas phase behavior of the Lennard-Jones system[14] as well as gas−liquid and liquid−liquid phase separation in binary mixtures.[21,41] Even very subtle features, such as the variation of the contact angle at triple phase coexistence, are obtained from accurate predictions of the underlying interfacial tensions. Bui and Cox have demonstrated the integration of the method in their work on charged systems.[18,22] Local learning gives access to neural hyperdensity functionals that are fit for making accurate predictions for the behavior of general observables.[16,42] The method also enables one to determine the individual values of the chemical potential across large data sets of inhomogeneous systems and using training data from mere canonical simulations is sufficient for local learning.[17]

The basic mechanism of local learning is to match the output of a neural network against simulation data for the one-body direct correlation function $c_1(\mathbf{r})$, where $\mathbf{r}$ denotes position. Results for $c_1(\mathbf{r})$ are readily available via simple postprocessing of sampling results for the density profile $\rho(\mathbf{r})$ obtained for a given form of the external potential $V_{\text{ext}}(\mathbf{r})$ and prescribed thermodynamic conditions. One then trains a neural network to either represent the one-body direct correlation *functional* $c_1(\mathbf{r}; [\rho])$ or the corresponding excess (over ideal gas) free energy functional $F_{\text{exc}}[\rho]$;[20] we indicate functional dependencies by square brackets. Both automatic differentiation and numerical functional line integration provide highly efficient tools to carry out flexible neural functional calculus. A pedagogical introduction to neural functional concepts is given in ref 38 using the one-dimensional hard rod system as a simple example; a corresponding tutorial is available online.[43]

Working with the direct correlation functionals is intimately connected with a force-based point of view; we recall that the one-body direct correlation functional yields the interparticle force field as the (scaled) gradient, $k_{\text{B}}T\nabla c_1(\mathbf{r}; [\rho])$, where ∇ denotes the derivative with respect to position $\mathbf{r}$, k_{B} is the Boltzmann constant and T absolute temperature. In *non-equilibrium* systems the interparticle force field depends in general on time t and the (causal) functional dependence is on both the dynamcial density profile $\rho(\mathbf{r}, t)$ and on the one-body current $\mathbf{J}(\mathbf{r}, t)$.[44] Hence the interparticle force functional $\mathbf{f}_{\text{int}}(\mathbf{r}, t; [\rho, \mathbf{J}])$ constitutes an appropriate target of the neural functional training.[45,46] Power functional theory provides the required unique functional relationships and an underlying exact minimization principle for the nonequilibrium dynamics.[44−54]

As local learning poses only very moderate demands on the compute load for producing the training data, the method was applied successfully in equilibrium by Kampa et al.,[15] in generalization of thermal training,[14,17,21] to one-dimensional fluids interacting with *arbitrary* short-ranged (truncated) pair potentials.[15] The neural training thereby encompasses both the density functional dependence on $\rho(x)$ as well as the 'metadensity' functional dependence on the form of the (scaled) pair potential $\beta\phi(r)$, where r denotes interparticle distance and $\beta = 1/(k_{\text{B}}T)$. Despite the rich heritage of analytical classical density functional research, very little is known systematically about the dependence on $\phi(r)$ beyond the simplest mean-field approximation, which is linear in $\phi(r)$. For bulk fluids this approximation is analogous to the random-phase closure that sets the bulk two-body direct correlation function $c_2^b(r) = -\beta\phi(r)$, see e.g., refs 55−58 for extensive discussion of background and applications to complex systems and e.g., refs 59−62 for work to generalize fundamental-measure concepts beyond hard core interactions.

Having access to a concrete neural representation of the metadensity functional for general pair interaction potentials opens up a range of exciting research perspectives, including addressing Henderson's inversion problem to determine uniquely the pair potential for given form of the pair distribution function,[63] as well as to address relevant questions of modern soft matter design.[15,64−66]

An alternative to local learning is the pair correlation matching method developed by Dijkman et al.[19,31] Their training strategy is based on using simulation results for bulk fluids only. Specifically, results for the radial distribution function $g(r)$ are generated (or are already known) for a range of bulk densities $\rho(\mathbf{r}) = \rho_b$ and are input into a numerical Ornstein−Zernike inversion scheme to obtain the corresponding bulk two-body direct correlation function $c_2^b(r; \rho_b)$. These results serve as the reference for the supervised training of their (convolutional) neural network that represents the excess free energy functional $F_{\text{exc}}[\rho]$. The training proceeds via pair-correlation matching the second density functional derivative of $F_{\text{exc}}[\rho]$, evaluated at *constant* bulk density, against the simulation results for $c_2^b(r; \rho_b)$.

Sammüller and Schmidt argue[20] that for *general* reliable density functional learning a more exhaustive exploration of the density function space, including also spatially inhomgenenous density profiles $\rho(\mathbf{r})$, should be beneficial and that this in particular is accomplished by the local learning method. They also argue that pair matching constitutes an efficient *regularizer* for local learning,[20] as the method operates on the two-body correlation level. The general machine learning concept of regularized learning refers to approaches that aim to improve model accuracy and generalization and these are often based on mere heuristics. In contrast, pair correlation regularization is motivated by physical first-principles and it has no adverse effect on the primary training goal of the neural functional.

Here we consider the concept of pair correlation matching in the light of the metadensity functional dependence on the pair potential. In the applications that we present, we restrict ourselves to one-dimensional fluids that interact via short-ranged (truncated) pair potentials that vanish beyond a fixed cutoff distance. We find this to be sufficient for our present conceptual investigation, as technical subtleties which arise in more general geometrical setups are avoided. However, we emphasize that our theoretical considerations are not restricted a priori to one-dimensional geometry; they rather continue to apply in higher-dimensional setups and we give a perspective on possible future applications in the outlook. We exploit the

https://doi.org/10.1021/acs.jpcb.6c01662
J. Phys. Chem. B XXXX, XXX, XXX−XXX

metadensity functional dependence on $\beta\phi(r)$ via its "metadirect" relationship with the bulk pair distribution function $g(r)$, as is given by functional differentiation of $F_{exc}[\rho, \beta\phi]$ via Evans' corresponding exact classical relationship.[3]

As a refined training method, we develop and validate a two-stage machine learning scheme where a primary metadensity functional[15] is used as a bootstrapping device for the generation of accurate neural results for the pair distribution function. This is based on test particle density functional minimization and it thus exploits Percus' concept[67] to set the external potential equal to the pair potential; see e.g., refs 68,69 for recent work. The corresponding physical situation is that of fixing one fluid particle at the origin and investigating the response on the surrounding system. Beyond merely obtaining $g(r)$ as an appropriately scaled version of the inhomogeneous density profile, thermodynamic differentiation of the neural density functional yields results for a corresponding locally resolved fluctuation profile. Then at the second training stage, these results are used to regularize the metadensity functional dependence on the pair potential. We demonstrate that the resulting regularized metadensity functional carries markedly reduced noise artifacts and we argue that it also has significant potential for systematic quantitative improvement over the nonregularized version.

The paper is organized as follows. We start in Section 2.1 by giving an overview of the required fundamentals of classical density functional theory in the light of the present context. Section 2.2 contains the essentials of the Ornstein−Zernike relationships for the two-body density, for the local compressibility, and for the behavior of the local fluctuation profiles associated with general observables. In Section 2.3 we lay out the formal consequences of the metadensity functional dependence on the pair potential. Section 3 contains a description of the neural functional learning method, including an overview of neural functional learning (Section 3.1), the description of the initial metadensity functional training (Section 3.2), and the neural generation of metadensity training data together with the details of the second-stage pair-correlation regularization (Section 3.3). Section 4 contains the presentation of our results for prototypical one-dimensional systems and in Section 5 we give conclusions.

2. METADENSITY FUNCTIONAL THEORY

2.1. Classical Density Functional Overview

We first lay out several formal aspects of the metadensity functional concept for the physics of classical fluids.[15] We start with an overview of classical density functional theory,[1,2] whereby we make the functional dependence on the interparticle interaction potential explicit. We consider systems that interact via a pair potential $\phi(r)$, where r is the interparticle distance. In general the system is exposed to an external potential $V_{ext}(\mathbf{r})$ and the thermodynamic statepoint is determined by the chemical potential μ and by temperature T.

The (thermally scaled) grand potential, when expressed as a functional of the one-body density $\rho(\mathbf{r})$, consists of the following sum

$$\beta\Omega[\rho, \beta\phi] = \beta F_{id}[\rho] + \beta F_{exc}[\rho, \beta\phi] + \int d\mathbf{r}\rho(\mathbf{r})[\beta V_{ext}(\mathbf{r}) - \beta\mu] \quad (1)$$

where the (thermally scaled) excess free energy functional $\beta F_{ext}[\rho, \beta\phi]$ depends on the one-body density profile $\rho(\mathbf{r})$ and on the scaled interparticle interaction potential $\beta\phi(r)$, as we have made explicit in the notation.

The ideal gas free energy functional is given explicitly by the following analytical expression:

$$\beta F_{id}[\rho] = \int d\mathbf{r}\rho(\mathbf{r})[\ln(\rho(\mathbf{r})\Lambda^d) - 1] \quad (2)$$

where Λ denotes the thermal de Broglie wavelength and d is the spatial dimensionality. The Mermin-Evans density functional minimization principle[1,2,6] ascertains that $\Omega[\rho, \beta\phi]$ is minimized in equilibrium and hence

$$\left.\frac{\delta\Omega[\rho, \beta\phi]}{\delta\rho(\mathbf{r})}\right|_{\rho=\rho_0} = 0 \text{ (min)} \quad (3)$$

where $\rho_0(\mathbf{r})$ denotes the equilibrium density profile. The corresponding equilibrium value of the grand potential, Ω_0, is obtained by evaluating the grand potential density functional (eq 1) at its minimum

$$\Omega_0 = \Omega[\rho_0, \beta\phi] \quad (4)$$

We drop the subscript of $\rho_0(\mathbf{r})$ for convenience in the following. The one- and two-body direct correlation functionals are given, respectively, as the first and second density functional derivatives of the (scaled) excess free energy functional $F_{exc}[\rho, \beta\phi]$ according to

$$c_1(\mathbf{r}; [\rho, \beta\phi]) = -\left.\frac{\delta\beta F_{exc}[\rho, \beta\phi]}{\delta\rho(\mathbf{r})}\right|_{\beta\phi} \quad (5)$$

$$c_2(\mathbf{r}, \mathbf{r}'; [\rho, \beta\phi]) = \left.\frac{\delta c_1(\mathbf{r}; [\rho, \beta\phi])}{\delta\rho(\mathbf{r}')}\right|_{\beta\phi} \quad (6)$$

Here the (thermally scaled) pair potential $\beta\phi(r)$ is kept fixed when differentiating functionally with respect to the density profile, as is standard and also implicit in the minimization condition (eq 3).

To obtain the excess free energy functional $\beta F_{exc}[\rho, \beta\phi]$, starting from the functional derivative (eq 5) yields the inversion via functional line integration[3,38]

$$-\beta F_{exc}[\rho, \beta\phi] = \int \mathcal{D}[\rho] c_1(\mathbf{r}; [\rho, \beta\phi]) \quad (7)$$

$$= \int d\mathbf{r}\rho(\mathbf{r}) \int_0^1 da c_1(\mathbf{r}; [a\rho, \beta\phi]) \quad (8)$$

In the rewriting (eq 8) we have expressed the formal density functional line integral (eq 7) via a specific and simple scaling parametrization that is straightforward to implement numerically in practice. The scaled density profile $a\rho(\mathbf{r})$ appears as the functional argument of the one-body direct correlation functional in the integrand of eq 8. The parameter range is $0 \le a \le 1$ according to the integration limits of the parametric integral. The (thermally scaled) pair potential $\beta\phi(r)$ is kept fixed when performing the functional line integral, as is consistent with the functional derivative (eq 5); see refs 3 and 38 for further background on functional line integration methods.

When working with neural functionals, the functional line integral (eq 8) was shown to yield accurate results e.g., for bulk thermodynamics[13] and for interfacial free energies.[14,21]

https://doi.org/10.1021/acs.jpcb.6c01662
J. Phys. Chem. B XXXX, XXX, XXX−XXX

Furthermore, the density functional derivatives (eqs 5 and 6) can be performed efficiently via automatic differentiation.[70,71]

Finally, inserting the grand potential decomposition (eq 1) into the minimization condition (eq 3) and carrying out the occurring functional derivatives yields the Euler−Lagrange equation

$$c_1(\mathbf{r};\,[\rho,\,\beta\phi]) = \ln(\rho(\mathbf{r})\Lambda^d) + \beta V_{\text{ext}}(\mathbf{r}) - \beta\mu \tag{9}$$

which is standard;[1−4] we set Λ to unity in the following. As before we have made the metadensity functional dependence on $\beta\phi(r)$ explicit in the notation on the left-hand side.

2.2. Generalized Ornstein−Zernike Relations

We give an overview of several recent generalizations of the classical two-body Ornstein−Zernike relation.[2,44] These extensions address the local compressibility,[72−76] the local thermal susceptibility,[76−78] and general fluctuation profiles that are associated with any chosen "hyperobservable" of interest.[16,42] Three key results are summarized: the standard inhomogeneous two-body Ornstein−Zernike relation,[1,2,44] the local compressibility one-body Ornstein−Zernike relation,[77−79] and the hyper-Ornstein−Zernike relation for general observables.[16,42] The latter case provides important background for the meta-Ornstein−Zernike relation[15] that we discuss below in Section 2.3. All equations of Ornstein−Zernike-type that we summarize below follow from appropriate differentiation of the fundamental Euler−Lagrange eq 9. As the respective derivatives are consistent with the statistical mechanical structure, these equations retain the exact nature of the Euler−Lagrange equation and hence of the underlying fundamental minimization principle (eq 3).

The inhomogeneous Ornstein−Zernike equation for a system with one-body density profile $\rho(\mathbf{r})$ is given by

$$h(\mathbf{r},\,\mathbf{r}') = c_2(\mathbf{r},\,\mathbf{r}') + \int \mathrm{d}\mathbf{r}''c_2(\mathbf{r},\,\mathbf{r}'')\rho(\mathbf{r}'')h(\mathbf{r}'',\,\mathbf{r}') \tag{10}$$

where the functional dependence of $c_2(\mathbf{r},\,\mathbf{r}'';\,[\rho,\,\beta\phi])$ on the density profile and on the scaled pair potential is suppressed in the notation. The standard two-body total pair correlation function is defined as $h(\mathbf{r},\,\mathbf{r}') = H_2(\mathbf{r},\,\mathbf{r}')/[\rho(\mathbf{r})\rho(\mathbf{r}')] - \delta(\mathbf{r} - \mathbf{r}')/\rho(\mathbf{r})$ with $H_2(\mathbf{r},\,\mathbf{r}') = \text{cov}(\hat{\rho}(\mathbf{r}),\,\hat{\rho}(\mathbf{r}'))$, where $\delta(\cdot)$ indicates the Dirac distribution. Here the covariance of two phase space functions $\hat{A}$ and $\hat{B}$ is defined in the standard way as $\text{cov}(\hat{A},\,\hat{B}) = \langle\hat{A}\hat{B}\rangle - \langle\hat{A}\rangle\langle\hat{B}\rangle$, where $\langle\cdot\rangle$ denotes the thermal equilibrium average, which we specify in detail below in Section 2.3. The one-body density operator has the standard form $\hat{\rho}(\mathbf{r}) = \sum_i \delta(\mathbf{r} - \mathbf{r}_i)$, where $\mathbf{r}_i$ denotes the position of particle $i = 1,...,N$. The two-body density is then defined as $\rho_2(\mathbf{r},\,\mathbf{r}') = \langle\hat{\rho}(\mathbf{r})\hat{\rho}(\mathbf{r}')\rangle - \delta(\mathbf{r} - \mathbf{r}')\,\rho(\mathbf{r})$.

The local compressibility $\chi_\mu(\mathbf{r})$ is a closely related one-body fluctuation profile,[73−81] which is defined by $\chi_\mu(\mathbf{r}) = \beta\,\text{cov}(\hat{\rho}(\mathbf{r}),\,N)$, such that $\chi_\mu(\mathbf{r}) = \beta\int \mathrm{d}\mathbf{r}' H_2(\mathbf{r},\,\mathbf{r}')$. The corresponding one-body fluctuation Ornstein−Zernike relation[77−79] for the local compressibility is given by

$$\frac{\chi_\mu(\mathbf{r})}{\rho(\mathbf{r})} = \beta + \int \mathrm{d}\mathbf{r}' c_2(\mathbf{r},\,\mathbf{r}')\chi_\mu(\mathbf{r}') \tag{11}$$

where $c_2(\mathbf{r},\,\mathbf{r}';\,[\rho,\,\beta\phi])$ is as before the two-body direct correlation functional.

In generalization of the local compressibility and the local thermal susceptibility,[76−78] for any given observable $\hat{A}$ the corresponding *hyperfluctuation* profile is $\chi_A(\mathbf{r}) = \text{cov}(\hat{\rho}(\mathbf{r}),\,\hat{A})$.[16,42] The following exact hyper-Ornstein−Zernike equation holds:[16,42]

$$\frac{\chi_A(\mathbf{r})}{\rho(\mathbf{r})} = c_A(\mathbf{r}) + \int \mathrm{d}\mathbf{r}' c_2(\mathbf{r},\,\mathbf{r}')\chi_A(\mathbf{r}') \tag{12}$$

where $c_A(\mathbf{r};\,[\rho,\,\beta\phi])$ is the one-body hyperdirect correlation functional and in the notation its functional dependence and that of $c_2(\mathbf{r},\,\mathbf{r}';\,[\rho,\,\beta\phi])$ on the density profile $\rho(\mathbf{r})$ and on the scaled pair potential $\beta\phi(r)$ are suppressed. We next examine closer the consequences of the latter "metadensity" functional structure.

2.3. Metadensity Functional Dependence

Metadensity functional theory[15] exploits the explicit functional dependence on the scaled pair potential $\beta\phi(r)$. We summarize several key points of the approach. The intrinsic free energy functional is the sum $F[\rho,\,\beta\phi] = F_{\text{id}}[\rho] + F_{\text{exc}}[\rho,\,\beta\phi]$, where we recall the explicit form (eq 2) of the ideal contribution and that $F_{\text{exc}}[\rho,\,\beta\phi]$ accounts for the interparticle interaction effects. The explicit Levy constrained search form[82,83] of the intrinsic free energy density functional is

$$\beta F[\rho,\,\beta\phi] = \min_{f\to\rho} \text{Tr} f(\beta H_{\text{int}} + \ln f) \tag{13}$$

where Tr · indicates the grand ensemble trace over all microscopic degrees of freedom and the constrained minimization is over those trial many-body distribution functions f that generate the given one-body density profile $\rho(\mathbf{r})$.[83] The integrand of the Levy form (eq 13) contains the intrinsic part of the Hamiltonian, which is defined as

$$H_{\text{int}} = \sum_i \frac{\mathbf{p}_i^2}{2m} + u(\mathbf{r}^N) \tag{14}$$

where the interparticle interaction potential $u(\mathbf{r}^N)$ depends on the position coordinates $\mathbf{r}_1,...,\mathbf{r}_N = \mathbf{r}^N$ of all N particles. For the case of only pairwise contributions this energy can be written as the following double sum

$$u(\mathbf{r}^N) = \frac{1}{2}\sum_{i=1}^{N}\sum_{j=1,j\neq i}^{N} \phi(|\mathbf{r}_i - \mathbf{r}_j|) \tag{15}$$

One may define a global measure of the pair distance distribution[15]

$$\hat{G}(r') = \frac{1}{2}\sum_{i=1}^{N}\sum_{j=1,j\neq i}^{N} \delta(r' - |\mathbf{r}_i - \mathbf{r}_j|) \tag{16}$$

which allows one to express the interparticle potential (eq 15) via integration over all distances r'

$$u(\mathbf{r}^N) = \int_0^\infty \mathrm{d}r'\hat{G}(r')\phi(r') \tag{17}$$

The thermal mean distribution of interparticle distances is then given as $G(r') = \langle\hat{G}(r')\rangle$, where the grand ensemble average is defined as $\langle\cdot\rangle = \text{Tr}\,\cdot f_0$ with f_0 denoting the grand ensemble equilibrium many-body probability distribution function. For completeness we spell out the explicit form $f_0 = \mathrm{e}^{-\beta(H-\mu N)}/\Xi$, with the grand partition sum $\Xi = \text{Tr}\,\mathrm{e}^{-\beta(H-\mu N)}$, and the full Hamiltonian $H = H_{\text{int}} + \sum_i V_{\text{ext}}(\mathbf{r}_i)$, where $V_{\text{ext}}(\mathbf{r})$ is the external potential and the sum is over all N particles.

When starting from the inhomogeneous two-body density distribution one can obtain $G(r')$ via integration: $G(r') = \int \mathrm{d}\mathbf{r}\int \mathrm{d}\mathbf{r}''\rho_2(\mathbf{r},\,\mathbf{r}'')\delta(r' - |\mathbf{r} - \mathbf{r}''|)/2$. As an alternative route, from

https://doi.org/10.1021/acs.jpcb.6c01662
J. Phys. Chem. B XXXX, XXX, XXX−XXX

the Levy definition (eq 13) of the intrinsic density functional one finds via functional differentiation

$$G(r';\,[\rho,\,\beta\phi]) = \left.\frac{\delta\beta F_{\mathrm{exc}}[\rho,\,\beta\phi]}{\delta\beta\phi(r')}\right|_{\rho} \tag{18}$$

$$= -\frac{\delta}{\delta\beta\phi(r')}\int \mathcal{D}[\rho]c_1(\mathbf{r};\,[\rho,\,\beta\phi])|_{\rho} \tag{19}$$

where the functional line integral form (second line) follows from writing out the excess free energy as the formal functional integral (eq 7). The identity is an equivalent rewriting of Evans' original result.[3] Exchanging the orders of functional differentiation and functional line integration yields

$$G(r';\,[\rho,\,\beta\phi]) = -\int \mathcal{D}[\rho]c_\phi(\mathbf{r},\,r';\,[\rho,\,\beta\phi])$$

$$= -\int \mathrm{d}\mathbf{r}\rho(\mathbf{r})\int_0^1 \mathrm{d}a c_\phi(\mathbf{r},\,r';\,[a\rho,\,\beta\phi]) \tag{20}$$

where the latter form is the standard (linear scaling) parametrization in density space. Thereby the "metadirect" correlation functional is defined as[15]

$$c_\phi(\mathbf{r},\,r';\,[\rho,\,\beta\phi]) = \left.\frac{\delta c_1(\mathbf{r},\,[\rho,\,\beta\phi])}{\delta\beta\phi(r')}\right|_{\rho} \tag{21}$$

As is indicated in the notation, the density profile is kept fixed upon building the functional derivative with respect to the scaled pair potential $\beta\phi(r')$.

As a simple illustration of the metadensity functional dependence, we consider the mean-field approximation $F_{\mathrm{exc}}^{\mathrm{MF}}[\rho] = \int \mathrm{d}\mathbf{r}\mathrm{d}\mathbf{r}'\rho(\mathbf{r})\rho(\mathbf{r}')\ \phi(|\mathbf{r}-\mathbf{r}'|)/2$, see e.g., refs 55−58 for applications to penetrable pair potentials and refs 72−76 for the treatment of interparticle attraction on top of (hard core) repulsion. The bilinear density functional dependence leads to the one-body direct correlation functional (eq 5) being linear in density, $c_1(\mathbf{r};\,[\rho,\,\beta\phi]) = -\int \mathrm{d}\mathbf{r}'\ \rho(\mathbf{r}')\ \beta\phi(|\mathbf{r}-\mathbf{r}'|)$. The corresponding form of the metadirect correlation functional (eq 21) follows as $c_\phi(\mathbf{r},\,r';\,[\rho]) = -\int \mathrm{d}\mathbf{r}''\ \rho(\mathbf{r}'')\ \delta(r'-|\mathbf{r}-\mathbf{r}''|)$. That this result is independent of $\beta\phi(r)$ is a feature of the mean-field approximation and will in general not hold.

One central role of the (formally exact) metadirect correlation functional (eq 21) is its appearance in the meta-Ornstein−Zernike relation,[15] which is exact and given by

$$\frac{\chi_\phi(\mathbf{r},\,r')}{\rho(\mathbf{r})} = c_\phi(\mathbf{r},\,r') + \int \mathrm{d}\mathbf{r}''c_2(\mathbf{r},\,\mathbf{r}'')\chi_\phi(\mathbf{r}'',\,r') \tag{22}$$

The functional arguments of $c_\phi(\mathbf{r},\,r';\,[\rho,\,\beta\phi])$ and of $c_2(\mathbf{r},\,\mathbf{r}'';\,[\rho,\,\beta\phi])$ have again been dropped for notational brevity. The metafluctuation profile $\chi_\phi(\mathbf{r},\,r')$ is a measure of the correlations between the local density and the global interparticle distance distribution, given by the following covariance

$$\chi_\phi(\mathbf{r},\,r') = -\mathrm{cov}(\hat{\rho}(\mathbf{r}),\,\hat{G}(r')) \tag{23}$$

The relationship of eqs 22 and 23 with the general hyper-Ornstein−Zernike relation eq 12 is via choosing the general hyperobservable to be $\hat{A} = -\hat{G}(r')$, see the definition (eq 16) of the pair distance observable $\hat{G}(r')$. This choice then leads to the exact identification $c_A(\mathbf{r}) = c_\phi(\mathbf{r},\,r')$ and $\chi_A(\mathbf{r}) = \chi_\phi(\mathbf{r},\,r')$.

It is natural to define also a global analog of the position-resolved metafluctuation profile (eq 23) in the following form

$$\chi_\phi^{\circ}(r') = \int \mathrm{d}\mathbf{r}\chi_\phi(\mathbf{r},\,r') = -\mathrm{cov}(N,\,\hat{G}(r')) \tag{24}$$

which follows from integrating eq 23 over position and noting that the total number of particles is $N = \int \mathrm{d}\mathbf{r}\ \hat{\rho}(\mathbf{r})$. In a bulk fluid, where the density profile is spatially constant, the metafluctuation profile is also spatially constant: $\rho(\mathbf{r}) = \rho_b \Rightarrow \chi_\phi(\mathbf{r},\,r') = \chi_\phi^b(r')$. We have the normalization relationship

$$\chi_\phi^b(r') = \chi_\phi^{\circ}(r')/V \tag{25}$$

where V is the sytem volume and for one-dimensional systems $V = L$ with system length L.

We next summarize several further relationships that are important for the neural training described later.

2.4. Consistency Relationships

The global distance distribution function $G(r)$, recall the definition (eq 16) of the corresponding observable $\hat{G}(r)$, is accessible via thermodynamic integration as follows

$$G(r;\,\mu) = -\beta\int_{-\infty}^{\mu}\mathrm{d}\mu'\int \mathrm{d}\mathbf{r}\chi_\phi(\mathbf{r},\,r;\,\mu') \tag{26}$$

In the notation we have indicated the dependence of the metafluctuation profile $\chi_\phi(\mathbf{r},\,r;\,\mu')$ on the chemical potential μ' as the integration variable and we have dropped the prime of the distance variable r for simplicity. The dependence on the thermodynamic variables μ, T arises from the average (eq 23). A proof of the relationship (eq 26) can be based on differentiating both sides with respect to μ, noting that $\partial G(r;\,\mu)/\partial\mu = -\beta\ \mathrm{cov}(N,\,\hat{G}(r))$, as can be seen by explicit calculation, and considering eq 24.

As laid out in Section 2.3 in a bulk fluid the metafluctuation profile is spatially constant, $\chi_\phi(\mathbf{r},\,\mathrm{r};\,\mu) = \chi_\phi^b(\mathrm{r};\,\mu)$, where

$$\chi_\phi^b(r;\,\mu) = -(\beta V)^{-1}\frac{\partial G(r;\,\mu)}{\partial\mu} \tag{27}$$

is the bulk "metacompressibility" and V denotes the system volume.

By rearranging the meta-Ornstein−Zernike relation (eq 22) one obtains for a bulk fluid

$$\chi_\phi^b(r;\,\mu) = \frac{c_\phi^b(r;\,[\rho_b,\,\beta\phi])}{\rho_b^{-1}-\tilde{c}_2^b(0)} \tag{28}$$

where $c_\phi^b(r;\,[\rho_b,\,\beta\phi])$ is the metadirect correlation functional (eq 21) evaluated at bulk fluid density ρ_b = const. Furthermore, $\tilde{c}_2^b(0) = \int \mathrm{d}\mathbf{r}c_2^b(|\mathbf{r}|)$ denotes the position integral over the bulk two-body direct correlation function $c_2^b(r)$. Our notation $\tilde{c}_2^b(0)$ is indicative of the limit of vanishing wavevector of the corresponding Fourier transform; see e.g., ref 14.

For one-dimensional bulk fluids, the relationship of $G(r)$ with the standard pair distribution function $g(r)$ is via simple normalization

$$G(r) = L\rho_b^2 g(r) \tag{29}$$

and for higher-dimensional systems appropriate geometric normalization is required.

For general inhomogeneous states, performing the integral of $G(r)$ over all distances r yields, from the definition (eq 16), the following thermal average

https://doi.org/10.1021/acs.jpcb.6c01662
J. Phys. Chem. B XXXX, XXX, XXX−XXX

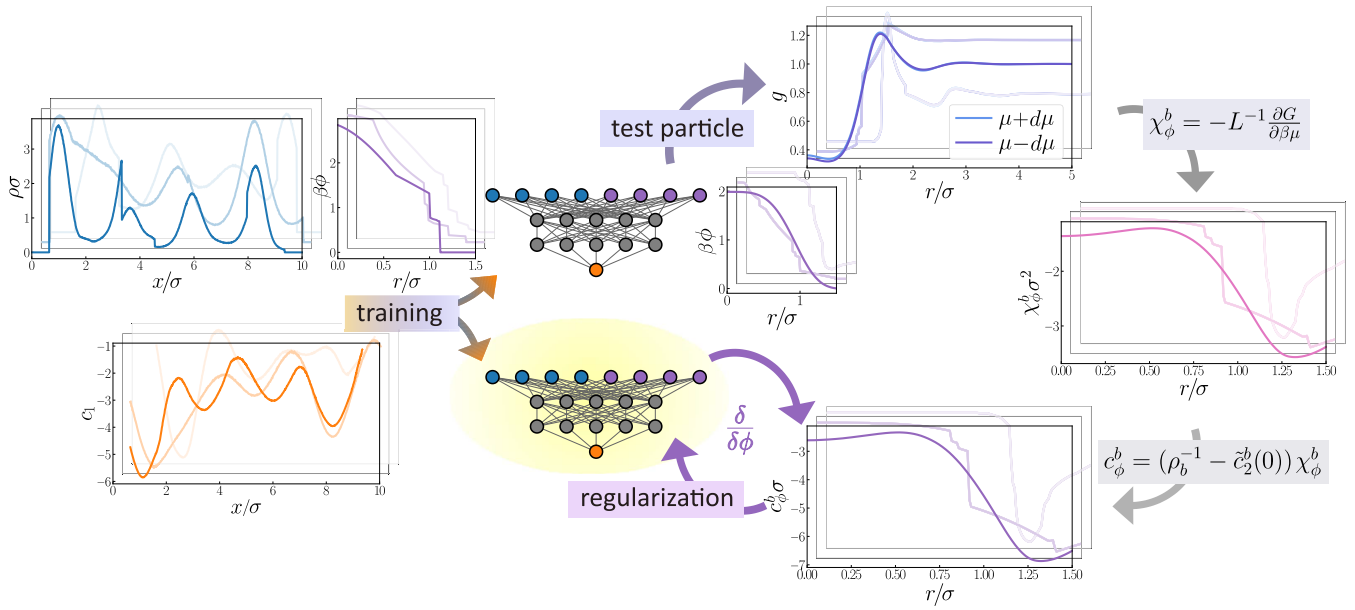

Figure 1. Overview of the two-stage neural functional learning (Section 3). From left to right: Training data consists of simulation results for inhomogeneous systems with density profiles $\rho(x)$ and interacting via short-ranged repulsive interparticle potentials $\phi(r)$ (Section 3.1). The corresponding one-body direct correlation functions $c_1(x)$ constitute the training target (Section 3.2). The initially trained neural functional $c_1(x; [\rho, \beta\phi])$ (top) is used in test particle setups for given forms of $\phi(r)$ to generate pair distribution functions $g(r)$ (Section 3.3). The corresponding bulk metafluctuation profile $\chi^b_\phi(r) = -L^{-1}\partial G(r)/\partial\beta\mu$ follows efficiently via considering finite differences $\mu \pm d\mu$. For the second training stage, the corresponding results for the bulk metadirect correlation function $c^b_\phi(r) = [\rho_b^{-1} - \tilde{c}^b_2(0)]\chi^b_\phi(r)$, see eq 37, are obtained. These are matched against those obtained via metadensity functional differentiation to regularize the second neural functional (bottom, highlighted), $c_\phi(x, r; [\rho_b, \beta\phi]) = \delta c_1(x; [\rho_b, \beta\phi])/\delta\beta\phi(r)$, see eq 21, where $c_\phi(x, r; [\rho_b, \beta\phi]) = c^b_\phi(r)$ is the matching condition (eq 38) that is independent of x due to the constant density profile. The second, regularized training stage thereby remains based also on local learning of the one-body direct correlation functional, as indicated. The background panels illustrate further representative training systems (not to scale).

$$\int_0^\infty \mathrm{d}rG(r) = \langle N(N-1)/2\rangle \tag{30}$$

which forms a useful sum rule to carry out consistency tests on data; in practice the upper integration limit ∞ is understood to indicate the integral over all distances that occur in the (finite) system volume.

The present theoretical framework sets the formal constraints and checks that are useful to set up and control the machine learning procedures, as described in the following.

3. METADENSITY FUNCTIONAL LEARNING

3.1. Overview of Local Functional Learning

We describe in the following how the theoretical metadensity functional structure (Section 2) can be exploited to significant effect when using simulation-based supervised machine learning to represent the functional relationships. The neural methodology rests on the straightforward availability of data for the direct correlation functions via simulations for a range of specific training systems. The training systems are constructed in a way that is as diverse as possible at the first learning stage, which in practice includes randomized thermodynamic conditions, randomized external potentials, and randomized pair potentials.[15]

Extracting the universal functional relationships from the training data is based on a neural network topology that acts as a mere universal approximator without any preconfigured internal structure. This is accomplished by using a standard fully connected multilayer perceptron. While we find this learning setup to be optimal for the current conceptual purposes, we see much potential for future progress in both tailoring the training data and the neural functional.[20]

We give a graphical overview of the supervised machine learning concept in Figure 1. The essential steps are the initial training of a neural metadensity functional (Section 3.2) and its use in the generation of *neural* training data which forms the basis for the second stage regularized training (Section 3.3).

3.2. Initial Metadensity Functional Training

At the first machine learning stage we use the setup described in ref 15 to train a neural one-body direct correlation functional $c_1(x; [\rho, \beta\phi])$ that makes the functional dependence on $\beta\phi(r)$ operational in practice. The method requires one to prepare a range of randomized training systems, which we identify by the index k, and to sample the corresponding density profile $\rho_k(x)$. Each training system k is specified by a corresponding randomized form of the external potential $V_{\mathrm{ext},k}(x)$, randomized values of the thermodynamical parameters μ_k and β_k, as well as a randomized form of (truncated) scaled pair potential $\beta_k\phi_k(r)$. (In practice, inverse temperature can be regarded as a constant scaling parameter.) A simple postprocessing step, based on the Euler−Lagrange eq 9, then yields simulation results for the one-body direct correlation function $c_{1,k}(x)$ for each training system as follows

$$c_{1,k}(x) = \ln \rho_k(x) + \beta_k V_{\mathrm{ext},k}(x) - \beta_k\mu_k \tag{31}$$

The local learning method aims to train a neural functional $c_1(x; [\rho, \beta\phi])$ such that equality between neural predictions and simulation results is achieved

$$c_1(x; [\rho_k, \beta_k\phi_k]) = c_{1,k}(x), \forall\ (x, k) \tag{32}$$

https://doi.org/10.1021/acs.jpcb.6c01662
J. Phys. Chem. B XXXX, XXX, XXX−XXX

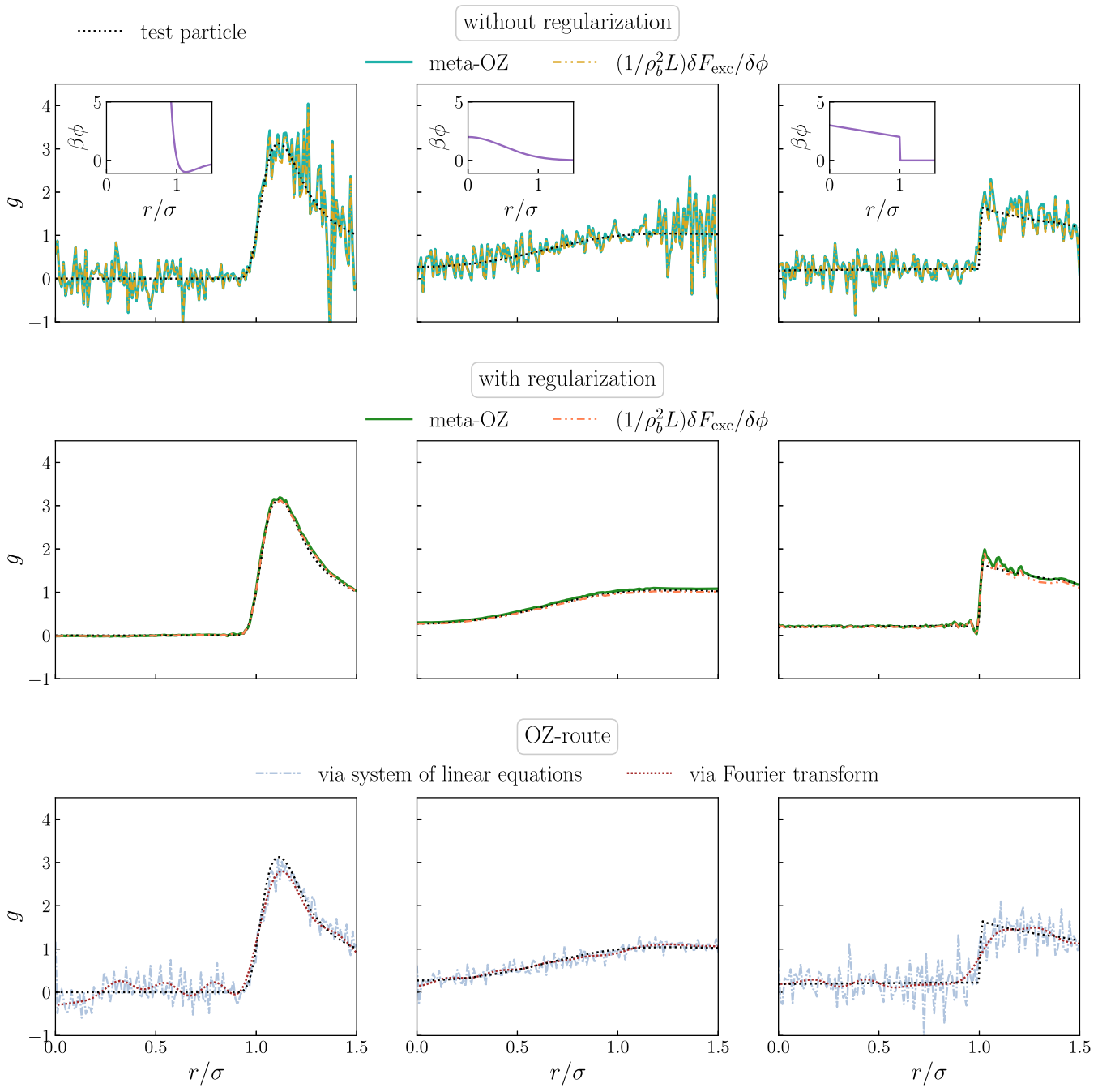

Figure 2. Neural functional results for the bulk pair distribution function $g(r)$ from different theoretical routes and from both unregularized and regularized metadensity functionals. The generality of both metadensity functionals is exemplified by their application to three different types of pair potentials (insets): truncated Lennard-Jones-like pair interaction (left column), repulsive Gaussian pair potential (middle column), and a penetrable-ramp potential (right column). The results for $g(r)$ are shown for scaled distances r/σ inside the pair potential window $r \leq r_c = 1.5\sigma$; the scaled chemical potential is $\beta\mu = 1$. In each panel the result from Percus' test particle minimization (solid line) serves as the reference; this route was found previously to yield excellent agreement with simulation data.[15] The results in the first row stem from a locally trained unregularized neural metadensity functional using either the meta-Ornstein−Zernike route (eqs 26, 28, and 29) or functional differentiation according to eqs 19 and 29: $(\rho_b^2 L)^{-1}\delta\beta F_{exc}[\rho, \beta\phi]/\delta\beta\phi(r)$ is evaluated numerically with stepwidth $d(\beta\phi) = 0.1$; see text. For each system both unregularized metadirect results exhibit irregular deviations from the (test particle) reference for $g(r)$, in particular for distances close to r_c and at the maximum of $g(r)$. The results in the second row are obtained using the pair-regularized neural metadensity functional following the same (metadirect) routes. Noise artifacts are eliminated and the agreement with the (test particle) reference is excellent. The results in the third row follow from using the standard density functional dependence instead of the metadensity channel of the neural functional. Numerical solution of the standard Ornstein−Zernike eq 10, using as input the bulk limit of eq 6, is performed either via solution of the corresponding set of linear equations, which arises upon spatial discretization of eq 10, or via spatial Fourier transform. While both routes predict qualitatively correct behavior, each one is prone to artificial numerical oscillation in regions of large scaled pair potential $\beta\phi(r)$ and to deviations near the first peak of $g(r)$.

The condition (eq 32) encapsulates the training goal to have the ouput of the neural functional (left-hand side) reproduce the 'target' simulation data (right-hand side). The matching should hold for all positions x in each training system k. As we

https://doi.org/10.1021/acs.jpcb.6c01662
J. Phys. Chem. B XXXX, XXX, XXX−XXX

restrict ourselves to interparticle potentials of finite range, we use a truncated density input "window" to represent the functional dependence of the neural one-body direct correlation functional;[13−15] we recall that the method remains useful when combined with insights[84,85] to treat additional long-ranged interparticle forces.[18,22,41]

3.3. Regularized Metadensity Functional Learning

Equation 32 is a sufficient condition for learning the functional dependence of $c_1(x)$ on both the density profile $\rho(x)$ and the scaled pair potential $\beta\phi(r)$, provided that the underlying functional mapping is adequately explored by the training data. In practice, however, it is useful to consider additional matching conditions both to alleviate the workload of generating a sufficient amount of training data and to improve the numerical quality of the neural network predictions. In the following, we lay out a workflow for incorporating radial distribution functions obtained from an initial ("unregularized") neural functional in the training of a second ("regularized") neural functional with the goal of improving its quality. The idea is simple: As metadensity functional theory facilitates multiple routes toward the pair correlation structure, enforcing consistency between different routes can be utilized as an additional matching condition for neural functional training. Ultimately, eq 38 will constitute this second matching condition and we lay out its first-principles origin in the following.

The unregularized neural metadensity functional (Section 3.2) is used to generate additional ("synthetic") training data for the following regularized learning. The generation of the training data proceeds via standard neural density functional minimization in test particle situations via numerical Picard iteration of the Euler−Lagrange eq 9. Test particle minimization is known to be an accurate method that is broadly applicable in a variety of contexts, including machine-learning,[35] fundamental-measure theory,[23,68] mean-field theory,[86] as well as for dynamics[44,53,87−92] and quantum physics.[93,94]

The test particle application of the neural metadensity functional theory yields results for pair correlation functions $g(r)$ for given forms of scaled pair potential $\beta\phi(r)$ as follows. In the Euler−Lagrange eq 9 one sets the external potential equal to the pair potential, $V_{\mathrm{ext}}(r) = \phi(r)$, and hence obtains

$$\rho_{\mathrm{g}}(r) = \exp(c_1(r; [\rho_{\mathrm{g}}, \beta\phi]) - \beta\phi(r) + \beta\mu) \tag{33}$$

which is a self-consistency equation that determines the density profile $\rho_{\mathrm{g}}(r)$ in the test particle geometry. The corresponding bulk density ρ_b = const can be obtained by self-consistent solution of the Euler−Lagrange eq 9 in absence of an external potential, $V_{\mathrm{ext}}(x) = 0$, which implies

$$\rho_b = \exp(c_1(r; [\rho_b, \beta\phi]) + \beta\mu) \tag{34}$$

Results for the pair distribution function $g(r)$ then follow by simple normalization

$$g(r) = \frac{\rho_{\mathrm{g}}(r)}{\rho_b} \tag{35}$$

Alternatively, one may obtain the bulk density ρ_b by using the limiting behavior of the test particle density profile at large distances, $\rho_{\mathrm{g}}(r) \to \rho_b$ for $r \to \infty$.

The high numerical accuracy that is attainable in the neural test particle minimization enables one to also obtain results for the bulk pair metafluctuation profile $\chi^b_\phi(r)$, as evaluated via the thermodynamical parametric derivative (eq 27) with the required results for $G(r)$ following from the rescaling (eq 29). Hence

$$\chi^b_\phi(r; \mu) = -\beta^{-1}\frac{\partial}{\partial\mu}\rho_b^2 g(r; \mu) \tag{36}$$

where the bulk density ρ_b depends on the value of the chemical potential μ, which needs to be taken into account when differentiating parametrically with respect to μ. Then from eq 28 one obtains the corresponding metadirect correlation function as

$$c^b_\phi(r) = [\rho_b^{-1} - \tilde{c}^b_2(0)]\chi^b_\phi(r) \tag{37}$$

In total, eqs 34−37 offer a fast and accurate means to obtain results for metadirect correlation functions $c^b_\phi(r)$ utilizing results from the test particle minimization (eq 33). Crucially, there are no simulations employed at this stage and the results are rather solely based on the (unregularized) neural functional described in Section 3.2. Its application to a range of randomized thermodynamic parameters μ_k, β_k and randomized (scaled) pair potentials $\beta_k\,\phi_k(r)$ hence generates an additional (synthetic) data set $c^b_{\phi,k}(r)$ to be used for metadirect regularization in a second training stage, as described in the following.

At the second training stage, our setup takes the concept of pair correlation matching,[19,31] which we recall was shown to be an efficient density functional regularizer,[20] and generalizes this for regularization of neural *metadensity* functionals. We thereby exploit the avenues offered by the explicit functional dependence on the scaled pair potential. Hence we use the following matching condition:

$$c_\phi(x, r; [\rho_{b,k}, \beta_k\phi_k]) = c^b_{\phi,k}(r) \tag{38}$$

where the left-hand side is the output of the neural metadirect correlation functional, obtained via automatic differentiation (eq 21). The right-hand side is the reference data obtained self-consistently, starting from test particle results for $g(r)$, which are converted via eq 36 to $\chi^b_\phi(r)$, which yield via eq 37 results for $c^b_\phi(r)$. Thereby the neural functional results for pair correlation functions $g(r)$ follow from test particle minimization using the purely locally trained neural functional as a bootstrapping device. In our notation we have retained in eq 38 the dependence on position x on the left-hand side; however, due to the density profile being spatially constant the neural functional output does not depend on the value of x.

4. RESULTS

We demonstrate numerically in the following that the regularized learning method described in Section 3 improves upon the 'bare' local metadensity functional learning[15] in terms of increased accuracy of the density functional results obtained via the "metachannel". We recall the overview of our machine learning strategy displayed in Figure 1, where real data were already shown.

In Figure 2 we display results for the bulk pair distribution function $g(r)$, as obtained via several different routes and for three different representative types of short-ranged pair potentials, namely a Lennard-Jones-like pair interaction, a repulsive Gaussian potential, and a penetrable-ramp form. The reference results are obtained from test particle minimization, as was shown previously to be numerically highly consistent

https://doi.org/10.1021/acs.jpcb.6c01662
J. Phys. Chem. B XXXX, XXX, XXX−XXX

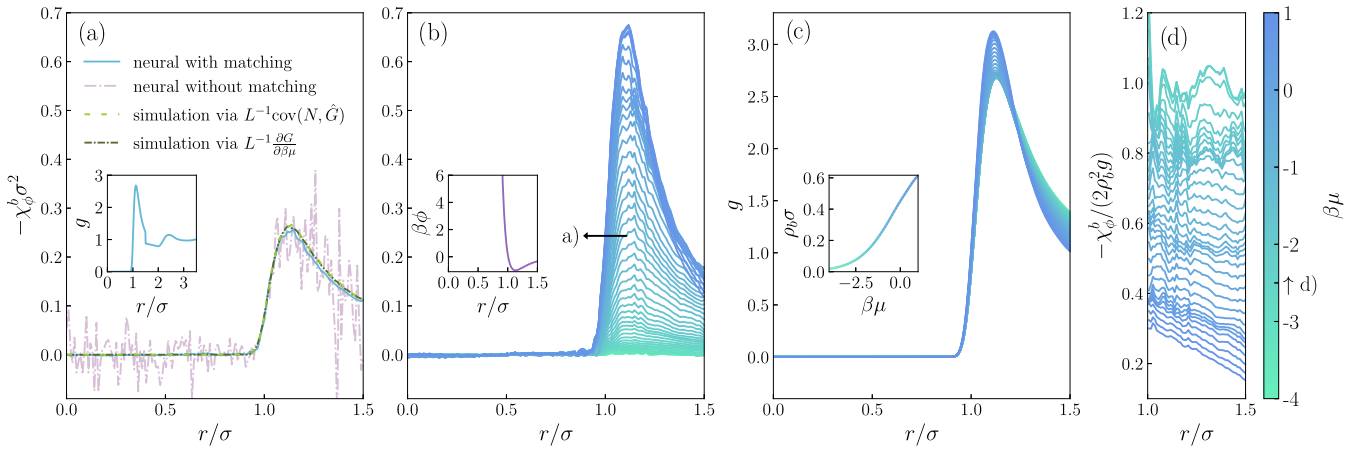

Figure 3. Illustration of the relationship of the bulk metacompressibility and the pair distribution function. (a) Scaled bulk metacompressibility, $-\chi_\phi^b(r)\sigma^2$, of a one-dimensional Lennard-Jones-like fluid at scaled chemical potential $\beta\mu = -1$ and pair distribution function $g(r)$ (inset). Results for $-\chi_\phi^b(r)\sigma^2$ are shown as a function of the scaled distance r/σ, obtained by solving the bulk meta-Ornstein−Zernike eq 28 using either the neural metadensity functional without or with regularization. Reference simulation data for system size $L = 5\sigma$ are obtained consistently by alternative methods: $-L^{-1}\partial G/\partial\beta\mu$ obtained from numerical differentiation of simulation results for $G(r)$ and spatial integration over sampled density covariance data according to $\chi_\phi^b(r) = -\int \mathrm{d}x\mathrm{cov}(\hat{\rho}(x), \hat{G}(r))/L$, which is identical to sampling the covariance $-\mathrm{cov}(N, \hat{G}(r))/L$. The expected equivalence of the results is reflected by their numerical agreement. (b) Variation of the scaled metafluctuation profile $-\chi_\phi^b(r)\sigma^2$, shown as a function of scaled interparticle distance r/σ, over a range of different values of the scaled chemical potential $\beta\mu$ (color bar). (c) Corresponding sequence of results for the pair distribution function $g(r)$, obtained via the test particle method. The inset shows the scaled bulk density $\rho_b\sigma$ as a function of $\beta\mu$ (inset). (d) Scaled ratio $\chi_\phi^b(r)/(2\rho_b^2 g(r))$ shown for distances outside the core, $1 < r/\sigma < 1.5$, and for $\beta\mu > -2.5$ (indicated by the vertical arrow at the colorbar). The low density limit of unity can be identified despite some noise artifacts and the thus scaled fluctuations are suppressed upon increasing bulk density.

with simulation data.[15] Having concrete access to the full metadensity functional dependence allows us to compare the results from a range of different routes to $g(r)$, including thermodynamic integration via eq 26 using either the unregularized or the regularized neural functional. The respective integrand is obtained via the bulk meta-Ornstein−Zernike eq 28 with all expressions on the right-hand side being evaluated via the neural metadensity functional. The results from the initial neural functional show qualitatively correct features, but they also display significant noise. In quite striking contrast, the results from the regularized functional show excellent agreement with the test particle reference (compare the first and second rows in Figure 2). Furthermore, calculating $F_{\mathrm{exc}}[\rho, \beta\phi]$ via functional line integration (eq 19) and differentiating the result with respect to $\beta\phi(r)$ gives very satisfactory agreement with the test particle data, serving as a valuable consistency check. We have performed this route, which is similar in spirit to the formal functional method described by Evans,[3] by using finite numerical differentiation. The value of the scaled pair potential $\beta\phi(r)$ at a chosen distance r is thereby increased by $d(\beta\phi) = 0.1$ and the resulting change in $F_{\mathrm{exc}}[\rho, \beta\phi]$ is monitored. Performing this finite differencing for all relevant values of r yields the full functional derivative.

Figure 2 also shows results from the numerical inversion of the homogeneous version of the Ornstein−Zernike eq 10 using as input the bulk two-body direct correlation function obtained via the density functional derivative (eq 6) evaluated at constant bulk density; see the bottom row of Figure 2. These results display quite pronounced oscillatory artifacts, which we attribute to the well-known numerical intricacy of reliable Ornstein−Zernike inversion rather than to a genuine shortcoming of the neural functional. Also results from solving the corresponding linear system of equations in real space are shown.

As further illustration of how the metachannel allows one to obtain the above results, we display in Figure 3 representative results for the scaled metafluctuation profile that forms the integrand in the thermodynamic integral (eq 26). Similarly to the one-body local compressibility $\chi_\mu(\mathbf{r})$, the metacompressibility profile $\chi_\phi^b(r)$ measures local fluctuations on the pair-correlation level. In test particle geometry, $\chi_\phi^b(r)$ and $\chi_\mu(r)$ are hence closely connected, cf. also their respective general covariance definitions given in eq 23 and above eq 11, which differ merely in the replacement of βN with $-\hat{G}(r)$. The results shown in Figure 3 are for a bulk fluid system of Lennard-Jones-like particles, see the inset in Figure 3 for a depiction of the form of $\beta\phi(r)$. As the benchmark we have carried out simulations, where sampling the covariance (eq 24) provides a viable means of determining $\chi_\phi^b(r)$. As a consistency check for the simulation reference, the comparison to the result from the alternative route via the thermodynamical derivative (eq 27) yields excellent confirmation. The neural functional results are obtained via the bulk version (eq 28) of the meta-Ornstein−Zernike relation (eq 22) and we reiterate that all quantities on the right-hand side follow from the same neural metadensity functional. In particular the input that creates the distance dependence is the metadirect correlation function $c_\phi^b(r)$, as is available from the functional derivative (eq 21) of $c_1(x; [\rho, \beta\phi])$ with respect to $\beta\phi(r)$, evaluated at constant bulk density. While the results obtained from the original functional indicate correct qualitative behavior, they also display significant scatter around the reference simulation data. In contrast, the regularized functional suffers from no such artifacts and displays excellent agreement with the simulation reference.

Figure 4 demonstrates the accessibility of the fully resolved metadirect correlation functional $c_\phi(x, r; [\rho, \beta\phi])$, we recall its definition (eq 21), in a representative inhomogeneous situation. The first panel depicts the highly inhomogeneous density profile $\rho(x)$ that emerges in response to the imposed

https://doi.org/10.1021/acs.jpcb.6c01662
J. Phys. Chem. B XXXX, XXX, XXX−XXX

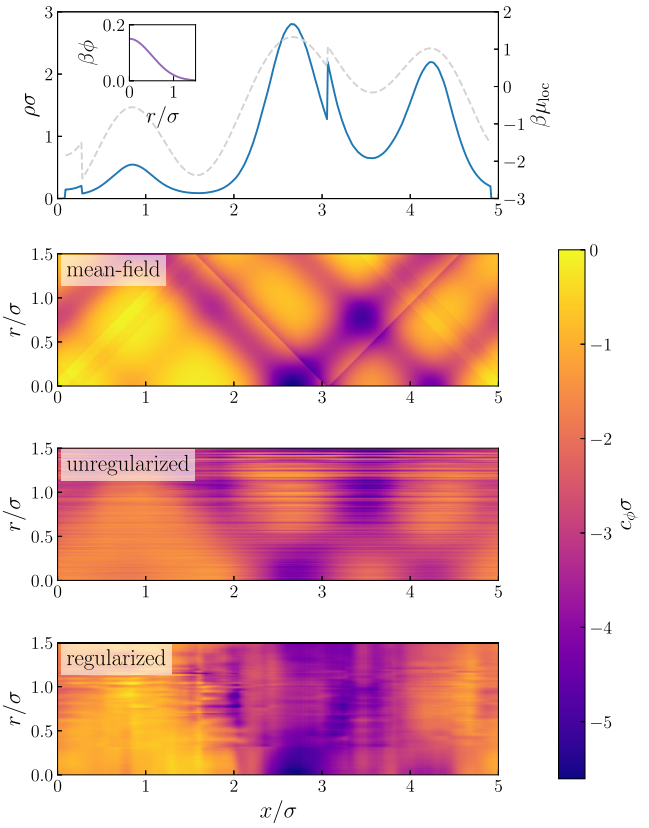

Figure 4. Illustration of the metadensity functional dependence in an inhomogeneous fluid with local chemical potential $\beta\mu_{\mathrm{loc}}(x) = \beta\mu - \beta V_{\mathrm{ext}}(x)$ and highly structured density profile $\rho(x)\sigma$ (top panel). The particles interact mutually with a repulsive penetrable pair potential (inset). The corresponding (scaled) metadirect correlation function $c_\phi(x, r)\sigma$, see eq 21, is shown as a function of (scaled) position x/σ and (scaled) interparticle distance r/σ. Three different functionals are used to generate results: the analytic mean-field approximation $\int \mathrm{d}x'\rho(x')\delta(|x' - x| - r)\sigma$ (second panel), as well as the unregularized (third panel) and regularized (bottom panel) neural one-body direct correlation functionals, which yield $c_\phi(x, r)$ via automatic differentiation according to eq 21.

external potential $V_{\mathrm{ext}}(x)$ and we have switched to a repulsive Gaussian interparticle potential to demonstrate the flexibility of the metadensity functional. For comparison we show the result obtained via the mean field approximation, $-\int \mathrm{d}x'\rho(x)\delta(r - |x - x'|)$, see the derivation given below eq 21. While the neural result shows qualitatively similar features, these are less pronounced, which we deem to be more realistic. The result obtained from the regularized functional shows reduced noise artifacts, but also a slightly more pronounced overall variation. From our general setup, we would expect this latter version to be the most accurate of the three.

We show in Figure 5 results for the two-body density and for the pair distance distribution $G(r)$ for a representative inhomogeneous situation. The density profile is sinusoidal and the particles interact again via Gaussian core repulsion. Grand canonical Monte Carlo simulations provide reference results for the two-body density distribution $\rho_2(x, x')$. We have ascertained that these results are consistent with the distance statistics, see the caption of Figure 5 for a detailed description. Solution of the inhomogeneous Ornstein–Zernike eq 10, where the neural functional provides input for $c_2(x, x')$, yields results for the two-body density that are in very good agreement with the simulation data.

5. CONCLUSIONS

In conclusion we have demonstrated that the metadensity functional dependence on the form of the thermally scaled pair potential $\beta\phi(r)$ provides fertile ground for deep and fresh insight into both the formal structure of classical density functional theory and the correlated equilibrium behavior of fluids. We have restricted our numerical work to one-dimensional systems that interact with range-truncated interparticle forces. The theoretical metadensity functional structure is general though and it holds, in principle, for higher spatial dimensions and for long-ranged pair potentials.

Our present contribution complements ref 15, where questions of Henderson inversion and inhomogeneous soft matter design were addressed for one-dimensional systems. These topics were shown there to connect naturally to the functional dependence on $\beta\phi(r)$.[15] Neural density functionals, obtained via the local learning strategy, allow one to capture accurately this "metadensity" functional dependence. In quite striking contrast, this feat is not currently possible analytically, as there is no generally applicable and reliable closed form for an excess free energy functional known. A makeshift is the simple mean-field approximation, where the dependence on $\phi(r)$ is linear, see the discussion below eq 21 and the comparison with the neural metadensity functional results presented in Figure 4. Tackling Henderson-type inversion problems requires an accurate description of the functional dependence on $\phi(r)$, which the neural metadensity functional can provide. In this regard, it remains to be scrutinized precisely for which conditions $\phi(r)$ can be determined uniquely from structural data in inhomogeneous settings; the neural metadensity functional can serve as valuable numerical guidance for this task.

Crucially, our results demonstrate that the neural dependence on the scaled pair potential $\beta\phi(r)$ transcends beyond being a mere input "switch" of the neural network. The 'metachannel' rather constitutes an accurate numerical representation of a formally well-defined and unique functional dependence, which we have in particular elucidated via Levy's constrained search method in Section 2.3 within the presentation of general concepts in Section 2. The data-driven evidence for the validity of the present functional point of view stems from the range of functional differentiation and functional line integral relationships that we could exploit consistently and confirm to be satisfied with high accuracy.

The present metadirect pair matching is to a certain extent inspired by the machine learning of classical density functionals via pair correlation matching as proposed by Dijkman et al.[19] These authors base their method on well-known statistical mechanical identities in density functional formulation to constrain and train their neural network. Specifically, the second density functional derivative of the excess free energy is matched against corresponding results for *bulk* two-body direct correlation functions. Importantly, Dijkman et al. considered the application of pair correlation matching to the truncated Lennard-Jones fluid only, with no possibility at inference stage to make predictions for other fluid types or for temperature values that are different from that used for training. Our present work expands upon this scheme in two important ways. One is the incorporation of training data for spatially *inhomogeneous* systems, which we deem to be essential for

https://doi.org/10.1021/acs.jpcb.6c01662
J. Phys. Chem. B XXXX, XXX, XXX−XXX

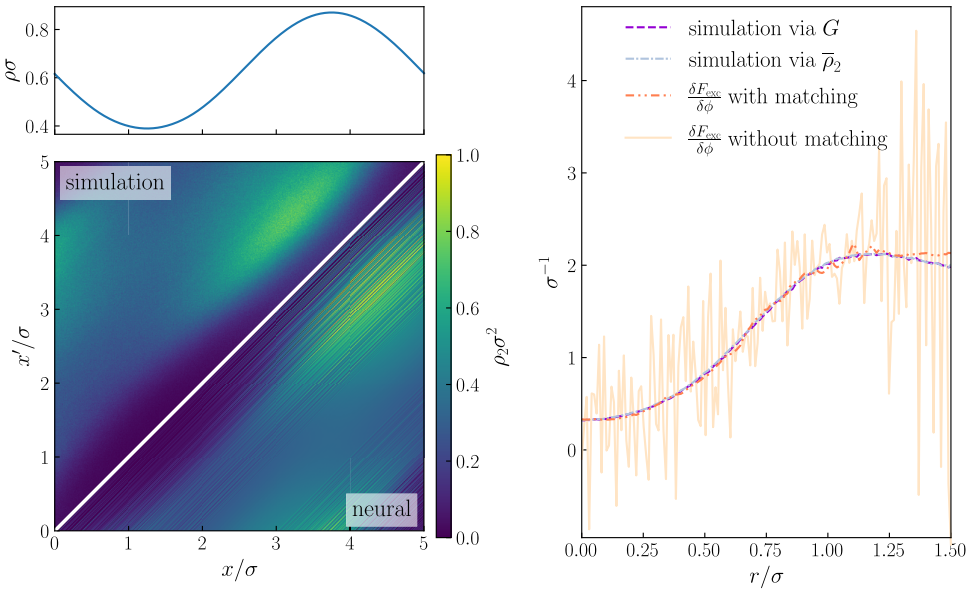

Figure 5. Demonstration of metadensity functional application in an inhomogeneous system. The particles interact via a repulsive Gaussian pair potential. The (scaled) one-body density profile $\rho(x)\sigma$ is sinusoidal (top left panel). Results for the scaled two-particle density $\rho_2(x, x')\sigma^2$ are shown as a function of x/σ and x'/σ and indicate structure formation (lower left panel). Simulation data is shown in the upper left triangle; the results in the lower right triangle are obtained from solving the inhomogeneous Ornstein−Zernike eq 10, using neural input for $c_2(x, x')$, and the consistency is reflected by the mirror symmetry around the counter-diagonal, $\rho_2(x, x') = \rho_2(x', x)$. The simulation results for $G(r)$ (right panel) are obtained either from sampling the interparticle distance histogram or, equivalently, by spatial integration $\overline{\rho}_2(r) = \int \mathrm{d}x \rho_2(x - r, x)$ with implied periodic continuation. The corresponding neural results are obtained via eq 19 using the unregularized or the regularized density functional.

reliable density functional learning; see the extensive discussion given in ref 20.

The second difference of our present approach to bulk pair correlation matching[19] is the depth at which the statistical mechanical structure is put to work. We recall that for fixed interparticle interaction potentials, thermal training[14,21] of neural functionals provides reliable access to temperature dependence and it allows one to predict accurately structure, thermodynamics, and the fluid phase behavior across varying control parameters. The metadirect functional dependence generalizes the mere parametric thermal dependence on β to the functional dependence on $\beta\phi(r)$, which incorporates both the (inverse) temperature parameter β as well as the form of the pair potential $\phi(r)$. As we have laid out in Section 2 the metadensity functional dependence allows one to put to work a range of classical formal results given by Evans.[3]

In particular we have constructed a regularized machine learning scheme that is based on the pair correlation structure obtained from functional differentiation with respect to the pair potential. We have dubbed this the "metadirect" route and this is accessible only due to the presence of the metachannel of the density functional and its amenability to functional calculus; see the introduction of the corresponding metadirect correlation functional in ref 15. We have described in detail in Section 3 how the metadensity dependence integrates itself into the local density functional learning and that a two-stage machine learning method forms an efficient and effective regularization scheme. We have exploited that these deep statistical mechanical roots can be integrated straightforwardly within modern computing paradigms of supervised neural network training and automatic differentiation. Together with fast neural functional line integration wide exploration and exploitation of the functional formulation is possible. It is in this sense that we put a variant of physics-informed machine learning to work via incorporation of statistical mechanical first principles. Although the supervised learning aspect remains based on simulation data, our present strategy differs from more common data-driven approaches that seek to represent a desired physical target quantity straight away by a surrogate model, see e.g., for a topical example the recent study by Liebchen and co-workers to learn the microstructure in active matter.[95]

As an outlook on potential future work, we mention several interesting topics. Instead of generating second-stage training data for metadirect pair matching self-consistently via the neural test particle procedure, one could alternatively use Monte Carlo results for the bulk metacompressibility profile. Albeit being more costly to obtain than the neural density functional results, this method could potentially avoid any latent "passing down" of inaccuracies from the first-stage neural functional. Related to this, how the bulk method by Dijkman et al.[19] would fare if generalized to include meta-dependence on the pair potential is an interesting question. Although only bulk states remain probed, incorporating the metadensity functional dependence should yield additional beneficial constraints on the resulting neural functional.

Interesting work could be aimed at elucidating the relationship of the bulk metacompressibility with the recent '3g'-sum rule[12] that connects $g(r)$ to two further (force−force and force-gradient) pair correlation functions. More generally, statistical mechanical gauge invariance[9−11] provides a powerful toolbox of formally exact sum rules that carry significant potential for the development of further physics-informed regularization schemes and for imposing concrete constraints on neural functionals.

While the results presented here attest to the prowess of the metadensity functional concept,[15] much important work remains to be addressed. All neural investigations in the present work concern one-dimensional systems of particles that interact via short-ranged (truncated) pair potentials. The

https://doi.org/10.1021/acs.jpcb.6c01662
J. Phys. Chem. B XXXX, XXX, XXX−XXX

metadensity dependence is only available within the finite input window size of $\beta\phi(r)$. Going beyond these limitations provides much fertile ground for future work. We believe that in particular taming spherically symmetric situations, which are a requirement for carrying out test particle calculations in $d > 1$, will be an important step to shed further light on the interrelationship of statistical mechanics and geometry. In this context relevant questions concerning the behavior at curved substrates, such as fluid adsorption and solvation effects, could be addressed from an arguably new angle. Our framework also ties in well with modern questions regarding the behavior of responsive colloids that adapt their interparticle interaction potential in response to various different stimuli and physical situations.[86,96−100] Addressing further generalizations to practically relevant types of soft matter, in particular to systems involving long-ranged interactions that arise e.g., in charged or dipolar fluids,[18,22] constitutes valuable future work.

■ ASSOCIATED CONTENT

Data Availability Statement

The data that support the findings of this article are openly available.[101]

■ AUTHOR INFORMATION

Corresponding Author

Matthias Schmidt − *Theoretische Physik II, Physikalisches Institut, Universität Bayreuth, D-95447 Bayreuth, Germany*; Email: Matthias.Schmidt@uni-bayreuth.de

Authors

Stefanie M. Kampa − *Theoretische Physik II, Physikalisches Institut, Universität Bayreuth, D-95447 Bayreuth, Germany*

Florian Sammüller − *Theoretische Physik II, Physikalisches Institut, Universität Bayreuth, D-95447 Bayreuth, Germany*; orcid.org/0000-0002-3605-329X

Complete contact information is available at: https://pubs.acs.org/10.1021/acs.jpcb.6c01662

Notes

The authors declare no competing financial interest.

■ ACKNOWLEDGMENTS

We thank Bob Evans for much inspiration to carry out this research, him and Jacco Dijkman for useful discussions, and the Special Issue Editors of J. Phys. Chem. B for their patience in receiving this article. This work is supported by the DFG (Deutsche Forschungsgemeinschaft) under project no. 551294732.

■ REFERENCES

(1) Hansen, J. P.; McDonald, I. R. *Theory of Simple Liquids*, 4th ed.; Academic Press: London, 2013.

(2) Evans, R. The nature of the liquid-vapour interface and other topics in the statistical mechanics of non-uniform, classical fluids. *Adv. Phys.* **1979**, *28*, 143−200.

(3) Evans, R. Density functionals in the theory of nonuniform fluids. In *Fundamentals of Inhomogeneous Fluids*; Henderson, D., Ed.; Dekker: New York, 1992. Chapter 3.

(4) Evans, R.; Oettel, M.; Roth, R.; Kahl, G. New developments in classical density functional theory. *J. Phys.: Condens. Matter* **2016**, *28*, No. 240401.

(5) Huang, B.; von Rudorff, G. F.; von Lilienfeld, O. A. The central role of density functional theory in the AI age. *Science* **2023**, *381*, 170−175.

(6) Mermin, N. D. Thermal properties of the inhomogeneous electron gas. *Phys. Rev.* **1965**, *137*, No. A1441.

(7) Baus, M. Broken symmetry and invariance properties of classical fluids. *Mol. Phys.* **1984**, *51*, 211−220.

(8) Henderson, J. R. Statistical mechanical sum rules. In *Fundamentals of Inhomogeneous Fluids*; Henderson, D., Ed.; Dekker: New York, 1992. Chapter 2.

(9) Hermann, S.; Schmidt, M. Noether's theorem in statistical mechanics. *Commun. Phys.* **2021**, *4*, No. 176.

(10) Müller, J.; Hermann, S.; Sammüller, F.; Schmidt, M. Gauge invariance of equilibrium statistical mechanics. *Phys. Rev. Lett.* **2024**, *133*, No. 217101.

(11) Müller, J.; Sammüller, F.; Schmidt, M. Why gauge invariance applies to statistical mechanics. *J. Phys. A: Math. Theor.* **2025**, *58*, No. 125003.

(12) Sammüller, F.; Hermann, S.; de las Heras, D.; Schmidt, M. Noether-constrained correlations in equilibrium liquids. *Phys. Rev. Lett.* **2023**, *130*, No. 268203.

(13) Sammüller, F.; Hermann, S.; de las Heras, D.; Schmidt, M. Neural functional theory for inhomogeneous fluids: Fundamentals and applications. *Proc. Natl. Acad. Sci. U.S.A.* **2023**, *120*, No. e2312484120.

(14) Sammüller, F.; Schmidt, M.; Evans, R. Neural density functional theory of liquid-gas phase coexistence. *Phys. Rev. X* **2025**, *15*, No. 011013.

(15) Kampa, S. M.; Sammüller, F.; Schmidt, M.; Evans, R. Metadensity functional theory for classical fluids: Extracting the pair potential. *Phys. Rev. Lett.* **2025**, *134*, No. 107301.

(16) Sammüller, F.; Robitschko, S.; Hermann, S.; Schmidt, M. Hyperdensity functional theory of soft matter. *Phys. Rev. Lett.* **2024**, *133*, No. 098201.

(17) Sammüller, F.; Schmidt, M. Determining the chemical potential via universal density functional learning. *Phys. Rev. Lett.* **2026**, *136*, No. 068202.

(18) Bui, A. T.; Cox, S. J. Learning classical density functionals for ionic fluids. *Phys. Rev. Lett.* **2025**, *134*, No. 148001.

(19) Dijkman, J.; Dijkstra, M.; van Roij, R.; Welling, M.; van de Meent, J.-W.; Ensing, B. Learning neural free-energy functionals with pair-correlation matching. *Phys. Rev. Lett.* **2025**, *134*, No. 056103.

(20) Sammüller, F.; Schmidt, M. Neural density functionals: Local learning and pair-correlation matching. *Phys. Rev. E* **2024**, *110*, No. L032601.

(21) Robitschko, S.; Sammüller, F.; Schmidt, M.; Evans, R. Learning the bulk and interfacial physics of liquid-liquid phase separation with neural density functionals. *J. Chem. Phys.* **2025**, *163*, No. 161101.

(22) Bui, A. T.; Cox, S. J. Dielectrocapillarity for exquisite control of fluids. *Nat. Commun.* **2026**, *17*, No. 2661.

(23) Cats, P.; Kuipers, S.; de Wind, S.; van Damme, R.; Coli, G. M.; Dijkstra, M.; van Roij, R. Machine-learning free-energy functionals using density profiles from simulations. *APL Mater.* **2021**, *9*, No. 031109.

(24) Kelley, M. M.; Quinton, J.; Fazel, K.; Karimitari, N.; Sutton, C.; Sundararaman, R. Bridging electronic and classical density-functional theory using universal machine-learned functional approximations. *J. Chem. Phys.* **2024**, *161*, No. 144101.

(25) Yatsyshin, P.; Kalliadasis, S.; Duncan, A. B. Physics-constrained Bayesian inference of state functions in classical density-functional theory. *J. Chem. Phys.* **2022**, *156*, No. 074105.

(26) Malpica-Morales, A.; Yatsyshin, P.; Duran-Olivencia, M. A.; Kalliadasis, S. Physics-informed Bayesian inference of external potentials in classical density functional theory. *J. Chem. Phys.* **2023**, *159*, No. 104109.

(27) Monti, E.; Yatsyshin, P.; Gkagkas, K.; Duncan, A. B. Learning density functionals to bridge particle and continuum scales. 2025, arXiv:2512.23840. arXiv.org e-Printarchive. https://arxiv.org/abs/2512.23840. (access date: April 15, 2026).

(28) Fang, X.; Gu, M.; Wu, J. Reliable emulation of complex functionals by active learning with error control. *J. Chem. Phys.* **2022**, *157*, No. 214109.
(29) Yang, J.; Pan, R.; Sun, J.; Wup, J. High-dimensional operator learning for molecular density functional theory. *J. Chem. Theory Comput.* **2025**, *21*, 5905−5915.
(30) Pan, R.; Fang, X.; Azizzadenesheli, K.; Liu-Schiaffini, M.; Gu, M.; Wu, J. Neural operators for forward and inverse potential-density mappings in classical density functional theory. *J. Chem. Phys.* **2025**, *163*, No. 164120.
(31) Ram, K.; Dijkman, J.; van Roij, R.; van de Meent, J.-W.; Ensing, B.; Welling, M.; Cremers, D. Learned free-energy functionals from pair-correlation matching for dynamical density functional theory. *Phys. Rev. E* **2025**, *112*, No. 045314.
(32) Santos-Silva, T.; Teixeira, P. I. C.; Anquetil-Deck, C.; Cleaver, D. J. Neural-network approach to modeling liquid crystals in complex confinement. *Phys. Rev. E* **2014**, *89*, No. 053316.
(33) Shang-Chun, L.; Oettel, M. A classical density functional from machine learning and a convolutional neural network,. *SciPost Phys.* **2019**, *6*, No. 025.
(34) Lin, S.-C.; Martius, G.; Oettel, M. Analytical classical density functionals from an equation learning network. *J. Chem. Phys.* **2020**, *152*, No. 021102.
(35) Glitsch, F.; Weimar, J.; Oettel, M. Neural density functional theory in higher dimensions with convolutional layers. *Phys. Rev. E* **2025**, *111*, No. 055305.
(36) Simon, A.; Belloni, L.; Borgis, D.; Oettel, M. The orientational structure of a model patchy particle fluid: simulations, integral equations, density functional theory and machine learning. *J. Chem. Phys.* **2025**, *162*, No. 034503.
(37) Simon, A.; Weimar, J.; Martius, G.; Oettel, M. Machine learning of a density functional for anisotropic patchy particles. *J. Chem. Theory Comput.* **2024**, *20*, 1062−1077.
(38) Sammüller, F.; Hermann, S.; Schmidt, M. Why neural functionals suit statistical mechanics. *J. Phys.: Condens. Matter* **2024**, *36*, No. 243002.
(39) Rosenfeld, Y. Free-energy model for the inhomogeneous hard-sphere fluid mixture and density-functional theory of freezing. *Phys. Rev. Lett.* **1989**, *63*, No. 980.
(40) Roth, R. Fundamental measure theory for hard-sphere mixtures: a review. *J. Phys.: Condens. Matter* **2010**, *22*, No. 063102.
(41) Zhou, K. L. Y.; Bui, A. T.; Cox, S. J. The roles of bulk and surface thermodynamics in the selective adsorption of a confined azeotropic mixture. *J. Phys. Chem. B* **2026**, *130*, 4455−4466.
(42) Sammüller, F.; Schmidt, M. Why hyperdensity functionals describe any equilibrium observable. *J. Phys.: Condens. Matter* **2025**, *37*, No. 083001.
(43) Sammüller, F. Neural functional theory for inhomogeneous fluids - Tutorial. https://github.com/sfalmo/NeuralDFT-Tutorial. (access date: April 15, 2026).
(44) Schmidt, M. Power functional theory for many-body dynamics. *Rev. Mod. Phys.* **2022**, *94*, No. 015007.
(45) de las Heras, D.; Zimmermann, T.; Sammüller, F.; Hermann, S.; Schmidt, M. Perspective: How to overcome dynamical density functional theory. *J. Phys.: Condens. Matter* **2023**, *35*, No. 271501.
(46) Zimmermann, T.; Sammüller, F.; Hermann, S.; Schmidt, M.; de las Heras, D. Neural force functional for non-equilibrium many-body colloidal systems. *Mach. Learn.: Sci. Technol.* **2024**, *5*, No. 035062.
(47) Fortini, A.; de las Heras, D.; Brader, J. M.; Schmidt, M. Superadiabatic forces in Brownian many-body dynamics. *Phys. Rev. Lett.* **2014**, *113*, No. 167801.
(48) Krinninger, P.; Schmidt, M.; Brader, J. M. Nonequilibrium phase behaviour from minimization of free power dissipation. *Phys. Rev. Lett.* **2016**, *117*, No. 208003.
(49) de las Heras, D.; Schmidt, M. Velocity gradient power functional for Brownian dynamics. *Phys. Rev. Lett.* **2018**, *120*, No. 028001.
(50) Stuhlmüller, N. C.; Eckert, T.; de las Heras, D.; Schmidt, M. Structural nonequilibrium forces in driven colloidal systems. *Phys. Rev. Lett.* **2018**, *121*, No. 098002.
(51) Hermann, S.; de las Heras, D.; Schmidt, M. Non-negative interfacial tension in phase-separated active Brownian particles. *Phys. Rev. Lett.* **2019**, *123*, No. 268002.
(52) de las Heras, D.; Schmidt, M. Flow and structure in nonequilibrium Brownian many-body systems. *Phys. Rev. Lett.* **2020**, *125*, No. 018001.
(53) Treffenstädt, L. L.; Schmidt, M. Universality in driven and equilibrium hard sphere liquid dynamics. *Phys. Rev. Lett.* **2021**, *126*, No. 058002.
(54) Renner, J.; Schmidt, M.; de las Heras, D. Shear and bulk acceleration viscosities in simple fluids. *Phys. Rev. Lett.* **2022**, *128*, No. 094502.
(55) Archer, A. J.; Evans, R. Binary Gaussian core model: Fluid-fluid phase separation and interfacial properties. *Phys. Rev. E* **2001**, *64*, No. 041501.
(56) Archer, A. J.; Likos, C. N.; Evans, R. Soft-core binary fluid exhibiting a λ-line and freezing to a highly delocalized crystal. *J. Phys.: Condens. Matter* **2004**, *16*, No. L297.
(57) Archer, A. J.; Chacko, B.; Evans, R. The standard mean-field treatment of inter-particle attraction in classical DFT is better than one might expect. *J. Chem. Phys.* **2017**, *147*, No. 034501.
(58) Archer, A. J.; Evans, R. Relationship between local molecular field theory and density functional theory for nonuniform liquids. *J. Chem. Phys.* **2013**, *138*, No. 014502.
(59) Schmidt, M. Density-functional theory for soft potentials by dimensional crossover. *Phys. Rev. E* **1999**, *60*, No. R6291.
(60) Schmidt, M. A density functional for additive mixtures. *Phys. Rev. E* **2000**, *62*, No. 3799.
(61) Schmidt, M. Fluid structure from density functional theory. *Phys. Rev. E* **2000**, *62*, No. 4976.
(62) Schmidt, M. Isometric and metamorphic operations on the space of local fundamental measures. *Mol. Phys.* **2011**, *109*, 1253−1263.
(63) Henderson, R. L. A uniqueness theorem for fluid pair correlation functions. *Phys. Lett. A* **1974**, *49*, 197−198.
(64) Coli, G. M.; Boattini, E.; Filion, L.; Dijkstra, M. Inverse design of soft materials via a deep learning-based evolutionary strategy. *Sci. Adv.* **2022**, *8*, No. eabj6731.
(65) Lindquist, B. A.; Jadrich, R. B.; Truskett, T. M. Communication: Inverse design for self-assembly via on-the-fly optimization. *J. Chem. Phys.* **2016**, *145*, No. 111101.
(66) Sherman, Z. M.; Howard, M. P.; Lindquist, B. A.; Jadrich, R. B.; Truskett, T. M. Inverse methods for design of soft materials. *J. Chem. Phys.* **2020**, *152*, No. 140902.
(67) Percus, J. K. Approximation methods in classical statistical mechanics. *Phys. Rev. Lett.* **1962**, *8*, No. 462.
(68) Gül, M.; Roth, R.; Evans, R. Using test particle sum rules to construct accurate functionals in classical density functional theory. *Phys. Rev. E* **2024**, *110*, No. 064115.
(69) Gül, M.; Roth, R.; Evans, R. Using test particle sum rules to improve approximations in classical density functional theory: White-Bear and White-Bear mark II versions of the Lutsko functional. *Phys. Rev. E* **2026**, *113*, No. 034104.
(70) Baydin, A. G.; Pearlmutter, B. A.; Radul, A. A.; Siskind, J. M. Automatic differentiation in machine learning: A survey. *J. Mach. Learn. Res.* **2018**, *18*, 1−43.
(71) Stierle, R.; Bauer, G.; Thiele, N.; Bursik, B.; Rehner, P.; Gross, J. Classical density functional theory in three dimensions with GPU-accelerated automatic differentiation: Computational performance analysis using the example of adsorption in covalent-organic frameworks. *Chem. Eng. Sci.* **2024**, *298*, No. 120380.
(72) Stewart, M. C.; Evans, R. Phase behavior and structure of a fluid confined between competing (solvophobic and solvophilic) walls. *Phys. Rev. E* **2012**, *86*, No. 031601.

https://doi.org/10.1021/acs.jpcb.6c01662
J. Phys. Chem. B XXXX, XXX, XXX−XXX

(73) Evans, R.; Stewart, M. C. The local compressibility of liquids near non-adsorbing substrates: a useful measure of solvophobicity and hydrophobicity? *J. Phys.: Condens. Matter* **2015**, *27*, No. 194111.
(74) Evans, R.; Stewart, M. C.; Wilding, N. B. A unified description of hydrophilic and superhydrophobic surfaces in terms of the wetting and drying transitions of liquids. *Proc. Natl. Acad. Sci. U.S.A.* **2019**, *116*, 23901−23908.
(75) Coe, M. K.; Evans, R.; Wilding, N. B. Density depletion and enhanced fluctuations in water near hydrophobic solutes: identifying the underlying physics. *Phys. Rev. Lett.* **2022**, *128*, No. 045501.
(76) Coe, M. K.; Evans, R.; Wilding, N. B. Measures of fluctuations for a liquid near critical drying. *Phys. Rev. E* **2022**, *105*, No. 044801.
(77) Eckert, T.; Stuhlmüller, N. C. X.; Sammüller, F.; Schmidt, M. Fluctuation profiles in inhomogeneous fluids. *Phys. Rev. Lett.* **2020**, *125*, No. 268004.
(78) Eckert, T.; Stuhlmüller, N. C. X.; Sammüller, F.; Schmidt, M. Local measures of fluctuations in inhomogeneous liquids: Statistical mechanics and illustrative applications. *J. Phys.: Condens. Matter* **2023**, *35*, No. 425102.
(79) Tarazona, P.; Evans, R. Long ranged correlations at a solid-fluid interface a signature of the approach to complete wetting. *Mol. Phys.* **1982**, *47*, 1033−1063.
(80) Coe, M. K.; Evans, R.; Wilding, N. B. Understanding the physics of hydrophobic solvation. *J. Chem. Phys.* **2023**, *158*, No. 034508.
(81) Wilding, N. B.; Evans, R.; Turci, F. What is the best simulation approach for measuring local density fluctuations near solvo/hydrophobes? *J. Chem. Phys.* **2024**, *160*, No. 164103.
(82) Levy, M. Universal variational functionals of electron densities, first-order density matrices, and natural spin-orbitals and solution of the v-representability problem. *Proc. Natl. Acad. Sci. U.S.A.* **1979**, *76*, 6062−6065.
(83) Dwandaru, W. S. B.; Schmidt, M. Variational principle of classical density functional theory via Levy's constrained search method. *Phys. Rev. E* **2011**, *83*, No. 061133.
(84) Cox, S. J. Dielectric response with short-ranged electrostatics. *Proc. Natl. Acad. Sci. U.S.A.* **2020**, *117*, 19746−19752.
(85) Bui, A. T.; Cox, S. J. A classical density functional theory for solvation across length scales. *J. Chem. Phys.* **2024**, *161*, No. 104103.
(86) Moncho-Jordá, A.; Goeth, N.; Dzubiella, J. Liquid structure of bistable responsive macromolecules using mean-field density-functional theory. *Soft Matter* **2023**, *19*, 2832−2846.
(87) Archer, A. J.; Hopkins, P.; Schmidt, M. Dynamics in inhomogeneous liquids and glasses via the test particle limit. *Phys. Rev. E* **2007**, *75*, No. 040501.
(88) Hopkins, P.; Fortini, A.; Archer, A. J.; Schmidt, M. The van Hove distribution function for Brownian hard spheres: Dynamical test particle theory and computer simulations for bulk dynamics. *J. Chem. Phys.* **2010**, *133*, No. 224505.
(89) Brader, J. M.; Schmidt, M. Power functional theory for the dynamic test particle limit. *J. Phys.: Condens. Matter* **2015**, *27*, No. 194106.
(90) Schindler, T.; Schmidt, M. Dynamic pair correlations and superadiabatic forces in a dense Brownian liquid. *J. Chem. Phys.* **2016**, *145*, No. 064506.
(91) Treffenstädt, L. L.; Schindler, T.; Schmidt, M. Dynamic decay and superadiabatic forces in the van Hove dynamics of bulk hard sphere fluids. *SciPost Phys.* **2022**, *12*, No. 133.
(92) Stopper, D.; Thorneywork, A. L.; Dullens, R. P. A.; Roth, R. Bulk dynamics of Brownian hard disks: Dynamical density functional theory versus experiments on two-dimensional colloidal hard spheres. *J. Chem. Phys.* **2018**, *148*, No. 104501.
(93) McCarty, R. J.; Perchak, D.; Pederson, R.; Evans, R.; Qiu, Y.; White, S. R.; Burke, K. Bypassing the energy functional in density functional theory: direct calculation of electronic energies from conditional probability densities. *Phys. Rev. Lett.* **2020**, *125*, No. 266401.
(94) Pederson, R.; Chen, J.; White, S. R.; Burke, K. Conditional probability density functional theory. *Phys. Rev. B* **2022**, *105*, No. 245138.
(95) Dasgupta, W.; Mandal, S.; Mukhopadhyay, A. K.; Liebchen, B. Learning microstructure in active matter. 2026, arXiv:2601.05894. arXiv.org e-Printarchive. https://arxiv.org/abs/2601.05894.(access date: April 15, 2026).
(96) Moncho-Jordá, A.; Dzubiella, J. Controlling the microstructure and phase behavior of confined soft colloids by active interaction switching. *Phys. Rev. Lett.* **2020**, *125*, No. 078001.
(97) Bley, M.; Dzubiella, J.; Moncho-Jordá, A. Active binary switching of soft colloids: stability and structural properties. *Soft Matter* **2021**, *17*, 7682−7696.
(98) Bley, M.; Hurtado, P. I.; Dzubiella, J.; Moncho-Jordá, A. Active interaction switching controls the dynamic heterogeneity of soft colloidal dispersions. *Soft Matter* **2022**, *18*, 397−411.
(99) Baul, U.; Dzubiella, J. Structure and dynamics of responsive colloids with dynamical polydispersity. *J. Phys.: Condens. Matter* **2021**, *33*, No. 174002.
(100) López-Molina, J.; Tirado-Miranda, M.; Dzubiella, J.; Moncho-Jordá, A. Density functional theory for responsive hard-sphere fluids. *Mol. Phys.* **2024**, *122*, No. e2410481.
(101) Code, data, and neural functionals. https://github.com/S-K-acc/meta-pair. (access date: April 15, 2026).

https://doi.org/10.1021/acs.jpcb.6c01662
J. Phys. Chem. B XXXX, XXX, XXX−XXX